JOURNAL OF ENDOUROLOGY
Volume 17, Number 7, September 2003

Cavitation Bubble Cluster Activity in the Breakage of Kidney Stones by Lithotripter Shockwaves

YURIY A. PISHCHALNIKOV, Ph.D.,[1] OLEG A. SAPOZHNIKOV, Ph.D.,[1] MICHAEL R. BAILEY, Ph.D.,[2] JAMES C. WILLIAMS, Jr., Ph.D.,[3] ROBIN O. CLEVELAND, Ph.D.,[4] TIM COLONIUS, Ph.D.,[5] LAWRENCE A. CRUM, Ph.D.,[2] ANDREW P. EVAN, Ph.D.,[3] and JAMES A. McATEER, Ph.D.[3]

ABSTRACT

***Background and Purpose*: There is strong evidence that cavitation bubble activity contributes to stone breakage and that shockwave–bubble interactions are involved in the tissue trauma associated with shockwave lithotripsy. Cavitation control may thus be a way to improve lithotripsy.**

***Materials and Methods*: High-speed photography was used to analyze cavitation bubble activity at the surface of artificial and natural kidney stones during exposure to lithotripter shockwaves *in vitro*.**

***Results*: Numerous individual bubbles formed on the surfaces of stones, but these bubbles did not remain independent but rather combined to form clusters. Bubble clusters formed at the proximal and distal ends and at the sides of stones. Each cluster collapsed to a narrow point of impact. Collapse of the proximal cluster eroded the leading face of the stone, and the collapse of clusters at the sides of stones appeared to contribute to the growth of cracks. Collapse of the distal cluster caused minimal damage.**

***Conclusion*: Cavitation-mediated damage to stones is attributable, not to the action of solitary bubbles, but to the growth and collapse of bubble clusters.**

INTRODUCTION

CAVITATION PLAYS AN IMPORTANT ROLE in shockwave lithotripsy (SWL). There is strong evidence that cavitation bubble activity contributes to stone breakage,[1–7] and recent studies support the idea that shockwave (SW)–bubble interactions are involved in the tissue trauma that occurs as a consequence of SW treatment.[8–13] The fact that cavitation appears to be linked both to stone breakage and to adverse effects has fueled interest in determining the precise mechanisms of bubble action and finding ways to control cavitation.

Several experimental findings help demonstrate the importance of cavitation in stone comminution. For example, placing a stone in a viscous medium[7,14,15] or covering the proximal face of the stone with a material that separates it from the surrounding fluid[14,16,17] reduces damage. Also, when stones are exposed to SWs at an overpressure sufficient to eliminate cavitation, they show no surface damage such as erosion or pitting, and the dose of SWs needed to fracture the stones is substantially increased.[2,17] In addition, when stones are treated with SWs for which the timing of the compressive and tensile components of the pressure pulse is reversed (thereby suppressing cavitation), damage is dramatically reduced.[11,18,19]

Cavitation control may be a way to improve lithotripsy. Studies with dual-SW sources have shown that timing of the lithotripter pulses can be used to suppress or intensify cavitation. If the second pulse arrives while cavitation bubbles initiated by the first pulse are growing ($\sim<100$ μsec), the bubble cycle is interrupted, and bubble collapse is weak. If, however, the second pulse arrives as bubbles are inertially collapsing ($\sim$250–300 μsec), bubble collapse is intensified, and bubble-mediated damage is increased. An obvious goal is to find conditions that enhance cavitation at the stone, and thus enhance stone breakage, but suppress cavitation within tissue—making

[1]Department of Acoustics, Physics Faculty, M.V. Lomonosov Moscow State University, Moscow, Russia.
[2]Center for Industrial and Medical Ultrasound, Applied Physics Laboratory, University of Washington, Seattle, Washington.
[3]Department of Anatomy and Cell Biology, Indiana University School of Medicine, Indianapolis, Indiana.
[4]Department of Aerospace and Mechanical Engineering, Boston University, Boston, Massachusetts.
[5]Division of Engineering and Applied Science, California Institute of Technology, Pasadena, California.

SW treatment more effective and safer. There has been good progress in this direction,[6,20–22] and work is ongoing to discover the potential of such strategies. One part of this effort is continued research to better characterize the mechanisms of SW–stone interactions to improve understanding of how cavitation bubbles cause damage.

Assessment of the role of cavitation in stone fragmentation is made difficult by the speed of the events. Shockwave propagation and cavitation bubble dynamics are fast processes, measured in nanoseconds (e.g., rise time of the shock front) to several hundred microseconds (e.g., inertial bubble collapse), so some events occur faster than conventional methods of detection can resolve. Still, very useful information about cavitation dynamics has been obtained even with methods that are limited to quantitation of the damage produced by bubble collapse. For example, the spatial extent and intensity of cavitation can be measured using aluminum foil targets.[23–25] Some temporal features of cavitation can be monitored by fiberoptic transmittance,[26,27] and the intensity of cavitation bubble collapse has been characterized by monitoring sonoluminescence.[28–30] Laser scattering methods[31,32] have been used to measure the time histories of bubble dynamics, and passive cavitation detection using single- or dual-focused hydrophones has been used to detect inertial cavitation both *in vitro* and *in vivo*.[5,9,12,28,33]

High-speed photography has been very useful for understanding how cavitation bubbles interact with stones. The first high-speed photographic observations of cavitation bubbles in the focus of a lithotripter provided dramatic visual evidence of the vast numbers of bubbles generated by each pressure pulse and confirmed the fact that bubbles indeed interact with the stone.[34] Since this initial report, various modes of high-speed photography have been utilized to study bubble activity. One method of capturing rapid events is to use pulsed-laser stroboscopic illumination with a conventional camera.[13,35,36] The drawback of such a set-up is that only one frame can be recorded per lithotripter pulse. Stroboscopic movies can be made by changing the laser pulse delay relative to the lithotripter spark discharge and recording numerous SWs. This approach has been used effectively to document bubble behavior in the free field,[37] to record the response of bubbles in a silicone-tubing blood vessel phantom,[13] and to capture simultaneously the SW stress fronts propagating within epoxy targets and profiles of the cavitation bubbles at the surface of these model stones.[36]

However, cavitation is not precisely repeatable from SW to SW.[28,33] Photographic reconstructions using the stroboscopic approach give a good estimate of cavitation but do not allow as extensive an appreciation of the dynamics of bubble activity as is possible by capturing multiple frames over the course of a single lithotripter pulse. That is, there is information to be gained from recording changes in bubble form and position from moment to moment.

One advantage to be gained from this approach is a better understanding of bubble interactions in lithotripsy. Almost all cavitation modeling in lithotripsy considers the behavior of single, spherical bubbles that remain symmetrical.[38–43] Some photographic studies have also focused primarily on the behavior of single bubbles in order to allow comparison with these models.[13,36,44,45] But cavitation in lithotripsy involves more than single bubbles, and this is evident regardless of the mode of image capture.[15,32,34,36,42] Bubble–bubble interactions in the form of "bubble clouds" and "bubble clusters" have a profound effect on cavitation dynamics in other systems,[46–50] and it seems likely that bubble cluster dynamics will prove to be important in lithotripsy as well.[51] Indeed, recent computations of bubble clouds generated by lithotripter pulses[52] have shown similarly dramatic effects, including strong dependence of shock focusing and collapse dynamics on bubble number density.

In the present paper, we report our observations using a high-speed multiframe camera to record cavitation at the surface of artificial and natural kidney stones *in vitro*. Sequential frames were captured to document the bubble activity generated by single SWs. The images show that cavitation at the surface of stones is in the form of bubble clusters and that violent cluster collapse contributes to stone breakage. These descriptive data should be useful as input for numerical modeling of bubble cluster collapse in SWL.

MATERIALS AND METHODS

High-speed camera

Images of cavitation bubbles at the surface of artificial and natural kidney stones were recorded using an Imacon-468 high-speed digital camera (DRS Hadland, Inc., Cupertino, CA). With this imaging system, seven 576 × 385-pixel frames could be recorded at speeds of up to 100 million frames per second. Interframe timing was adjustable (minimum 10 nsec). Lighting was provided by a single high-intensity xenon flash lamp of 1.5-msec duration with 1000 J of stored energy. Triggering was achieved using a photodiode to detect the light from the lithotripter spark discharge. Digital images were post-processed using Adobe Photoshop. Each image was adjusted using Auto Levels and sharpened using the Unsharp Mask filter (amount = 100%; radius = 4 pixels). More than 300 high-speed sequences (seven frames each) of bubble behavior at the surface of stones were recorded and analyzed by this method.

Lithotripter

Studies were conducted using a research electrohydraulic lithotripter that produces the same acoustic output as an unmodified Dornier HM3 clinical lithotripter (80-nF capacitor).[53] Electrohydraulic lithotripters employ an underwater spark discharge to produce a shock pulse. The spark discharge takes place at the internal focus (F_1) of an ellipsoidal reflector, which focuses the SW to an external focal point (F_2). The ellipsoidal reflector of the research lithotripter had the same dimensions as that of the Dornier HM3: major half-axis $a = 139$ mm and minor half-axis $b = 78$ mm. The travel distance of the SW from the spark to the reflector and on to F_2 was $2a = 278$ mm. Assuming the speed of sound in water to be 1500 m/sec, the corresponding time delay for this travel distance (i.e., spark source to target) is 185 μsec.

The temporal profile of the shock pulse produced by our lithotripter has been characterized using a calibrated PVDF membrane hydrophone and consists of a positive spike with a shock front followed by a negative tail, all with a total duration of ~4 μsec.[53] The experiments described in the present study were performed at a charging potential of 20 kV. At this potential, the lithotripter pulse had a peak positive-pressure am-

plitude of ~40 MPa and a peak negative-pressure amplitude of ~8 MPa. The −6-dB zone of the acoustic field of this lithotripter measured ~10 mm wide × ~60 mm axial length.

The lithotripter water tank had an optically clear glass window on a cylindrical port that extended inward, making it possible to position the lens of the high-speed camera within 100 mm of F_2. This did not alter the acoustic field. For all experiments, the tank was filled with degassed water softened by addition of $NaHCO_3$ (conductivity ~660 μS/cm). Filtered (100-μm filter) deionized water was degassed under vacuum in a closed system for 1 to 2 hours prior to placement in the lithotripter tank. For these experiments, water was held in the lithotripter for 4 to 6 hours without further degassing. The oxygen content of the water increased during this time from ~3 to 4 ppm at time of filling of the lithotripter to no greater than 5.5 ppm at completion of experiments. Thus, dissolved gas and cavitation nuclei were never completely removed from the lithotripter water.

Artificial and natural stones

Two types of artificial stones prepared from gypsum cement were used. Ultracal 30™ (U-30) gypsum (United States Gypsum Company, Chicago, IL)[54] or Portland cement was mixed with deionized water (U-30 1:1; Portland 1:3). The mixture was pipeted into flat-bottom 96-well polystyrene cell culture plates (No. 3596; Costar, Cambridge, MA) and allowed to solidify under water overnight. The plastic was dissolved with chloroform to release the pellets. The stones were washed thoroughly with water and stored under water. The U-30 stones measured approximately 6.5 × 7.5 mm. The density, longitudinal, and transverse wave velocities for U-30 stones were $\rho = (1.7 \pm 0.1) \times 10^3$ kg/(m^3), $c_l = (3.1 \pm 0.3) \times 10^3$ m/sec, and $c_t = (1.5 \pm 0.3) \times 10^3$m/sec, respectively, which is in the range found with natural stones.[55] We have used U-30 cylinders previously as model stones to assess the damage mechanisms of lithotripter SWs.[17,56–58] The stones made from Portland cement measured approximately 6.5 × 10 mm.

Natural calcium oxalate monohydrate kidney stones were obtained from a urinary stone analytical service (Beck Analytical Services, Indianapolis, IN). Prior to use, these stones were hydrated by submersion in water for 10 days. For lithotripsy, stones were either placed atop a sheet of 4-mil low-density polyethylene or were held by a household rubber band. All image sequences show bubble activity generated by a single SW. Throughout the course of these experiments, numerous recordings were made using a given stone, and, typically, the single SWs were fired minutes apart. In some cases (where specifically noted), the images capture the cavitation associated with the last of a series of SWs fired at a predetermined rate.

RESULTS

Bubble clusters at the stone surface were derived from individual bubbles

Analysis of sequential frames showed that the development of bubble clusters was preceded by the formation of individual bubbles. Figure 1 presents a series of frames in which the first image shows the stone at 180 μsec, just at the time of arrival of the SW and before bubbles are visible. At 250 μsec (Fig. 1B), the stone is covered by numerous small bubbles. As seen in subsequent frames, these bubbles grow and aggregate to form a cluster that overlies most of the surface of the stone. Many of the individual bubbles seen earlier are no longer identifiable. The coalescence of bubbles—the recruitment of individual bubbles into a cluster—is suggested as well (Fig. 1E, F; see also Figs. 7 and 8 below) in which movement of the bubble cluster across the surface of the stone leaves portions of the stone bub-

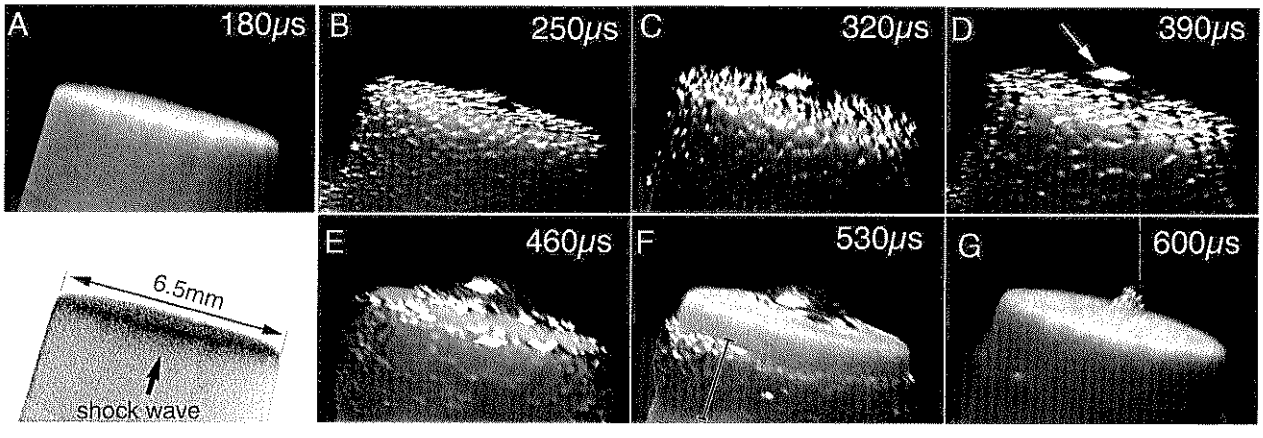

FIG. 1. Individual cavitation bubbles contributing to formation of bubble clusters on surface of artificial stone. This series of frames, captured in 70-μsec steps, shows cavitation bubble activity generated by single lithotripter pulse. Images focus on distal third of stone. Axis of SW propagation was nearly vertically upward (see inset). (**A**) Stone at time of SW arrival but prior to formation of cavitation bubbles. (**B**) At 70 μsec after passage of SW, numerous individual cavitation bubbles have formed on surface of stone. (**C, D**) Bubbles have enlarged and begun to coalesce into cluster. Prominent bubble (arrow) is visible at center of distal surface of stone. (**E**) Portion of bubble cluster has begun to move from end of stone to lateral surface. (**F**) Bubbles have divided into two separate clusters: one possibly single bubble at center of distal end of stone and one (I) forming ring or band that appears to encircle stone. (**G**) Both distal bubble and cluster along sides of stone have collapsed.

ble free. That is, the images give the impression that individual bubbles have become caught up in the cluster and have moved from their original position.

Bubble clusters occurred reproducibly across several regions of the stone

For the majority of experiments, cylindrical stones were used and were positioned so that their long axis was along the acoustic axis of the lithotripter. With this orientation, the stone presented a flat proximal end or face, curved sides, and a flat distal end. The incoming SW thus hit the flat proximal end first (Fig. 2A). With each lithotripter pulse, there was, consistently, the formation of a population of individual bubbles that then gave rise to three main bubble clusters: one at the proximal face, one at the distal end, and one along the sides of the stone. The bubble cluster at the proximal face (proximal cluster) (Figs. 2 and 3) typically formed an envelope or blister that, as it expanded, extended as much as 3 mm from the surface of the stone. It would then constricted close to its point of contact with the stone (Figs. 2F and 3) and took on a "mushroom cloud" shape. The cluster collapsed to a narrow (~2-mm) point of impact near the center of the stone and then rebounded (Fig. 4). It was this region of the proximal face that, on treatment with multiple SWs, showed damage in the form of a crater or pit (Fig. 5A). The remainder of the proximal face was relatively undamaged. Thus, the formation and subsequent collapse of the bubble cluster at the proximal face of the stone appears to have involved the coalescence of numerous individual cavitation bubbles to form a large single bubble or cluster of bubbles that collapsed with damaging force.

Concurrent with the formation of the proximal bubble cluster, another cluster developed at the distal end of the stone (Figs. 1 and 6), and still another formed along the sides of the stone (Figs. 7 and 8). The distal cluster was the smallest of the three in overall area and remained centered atop the distal end of the stone. This cluster sometimes appeared to be a solitary bubble (Figs. 1F; 6E, F) that collapsed sooner than the proximal cluster (duration of distal cluster ~400 μsec; proximal cluster ~600 μsec) and caused very little damage to the distal end of the stone (Fig. 5B).

The cluster associated with the sides of the stone exhibited substantial movement as it retracted from the distal end and over the edge and down the sides of the stone (Figs. 1F, 6C–F, 7D, E, 8D, E). Following retraction to the side of the stone, this cluster formed a band or ring that appeared to extend completely around the stone (Figs. 1F, 7E, and 8E) and collapsed to a narrow line. Although some high-speed camera images (Figs. 1G

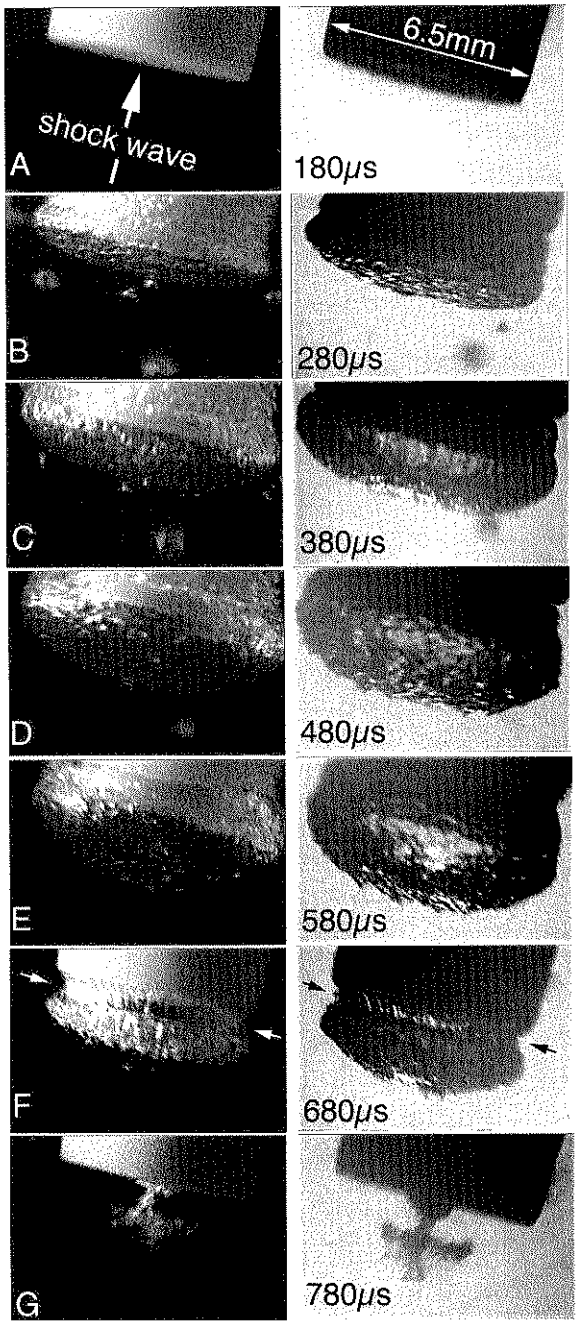

FIG. 2. Bubble cluster formation and collapse on proximal face of stone. These images, captured in 100-μsec steps, show growth of bubble cluster that consistently formed on leading face of stone. Two different stones are shown, and images were recorded using illumination from different points: from side for images in left column and from back for images in right column. With side lighting, stone is light, and bubbles are transparent; with back lighting, stone is dark, and bubbles are opaque. (**A**) Stone at time of SW arrival, before cavitation bubbles have formed. Arrow shows direction of pulse propagation. (**B–D**) Formation and growth of cluster over leading face of stone. With side lighting (left), one can see numerous small bubbles on surface of stone and caught up by expanding cluster. With back lighting (right), surface of cluster appears rough. (**E**) Cluster has now expanded to extend ~3 mm off surface of stone. With side lighting (left), one can see that bubble both overlaps edge of stone and extends up the sides. It is difficult in either frame to resolve individual bubbles within cluster. (**F**) Cluster has begun to collapse: it has retracted from sides of stone and is constricted at its base (arrows). (**G**) Cluster has collapsed at center of proximal face of stone. Note: Time from impact of SW to initial collapse of proximal cluster was approximately 600 μsec. Cavitation cycle for individual bubbles in surrounding water is approximately 300 μsec.[42,65]

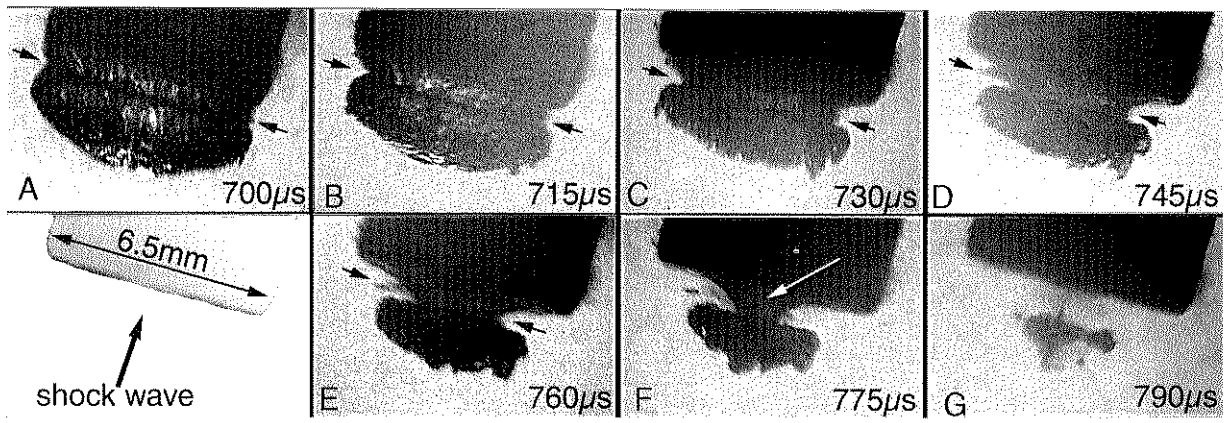

FIG. 3. Details of bubble cluster collapse on proximal face of stone. This series of images shows 15-μsec steps beginning 700 μsec after spark discharge and therefore corresponds approximately to interval between panels F and G of Figure 2. Collapse times of bubble clusters in Figures 2 and 3 differ slightly: this is typical of shot-to-shot variability in shock pulse amplitude that has been documented for electrohydraulic lithotripters.[28,33] (**A–E**) Bubble cluster constricts at its base (black arrows), while dome or cap gets smaller at slower rate. (**F**) Cluster now consists of cap and narrow stalk (white arrow), with stalk centered over proximal face of stone. (**G**) Stalk is no longer visible, and only portion of cluster cap remains. Faint shadow between stone and cluster may be debris eroded from stone by impact from collapse of cluster.

and 8G) give the impression that sand was dislodged from the stone, collapse of this side cluster did not result in erosion or pitting. Clusters at the side of the stone also appeared to coalesce with and contribute to the cluster at the proximal end of the stone. Figures 2, 9, and 11 show cases where bubbles below the level of the rubber band swept down to join the proximal cluster.

The occurrence of a bubble cluster at the side of the stone was a consistent feature observed for each SW and did not appear to be influenced by the way in which the stone was held in the lithotripter. That is, in most experiments, the stones were held in position by a rubber band. However, clusters did not consistently develop in contact with the rubber band and, indeed, formed on stones that were supported by a sheet of low-density polyethylene instead of being secured by a rubber band (Fig. 8).

Cavitation bubble clusters along sides of stones interacted with fractures

Cracks perpendicular to the SW axis commonly developed in the target stones during SW treatment (Figs. 9–12). The fracture line was usually 2 to 3 mm from the distal end and, thus, in a position characteristic of failure by a spall mechanism.[7,59–61] Cracks appeared to attract bubble cluster activity. It may not always have been possible to see fractures in the recorded images, but when a fracture was observable, it typically marked the site of collapse of the side cluster. That is,

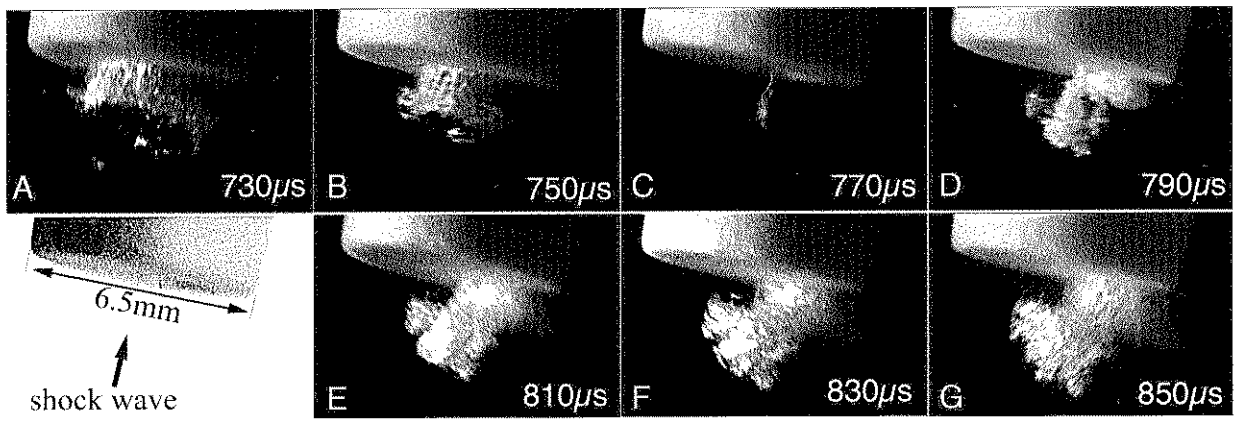

FIG. 4. Cavitation bubble rebound following cluster collapse on proximal face of stone. Frames were captured in 20-μsec steps, and first frame corresponds to approximately the same point in development of proximal bubble cluster as Figure 3C. (**A, B**) Cluster is collapsing slightly off center. (**C**) Collapse is nearly complete; just wisp of cluster remains. (**D–G**) Rebounding cluster grows outward. It is difficult to identify debris that might be carried within cluster. Note: This figure shows last of series of 10 SWs delivered at rate of 5 Hz. Bubble cluster formation, growth, collapse, and rebound were observed regardless of pulse-repetition frequency.

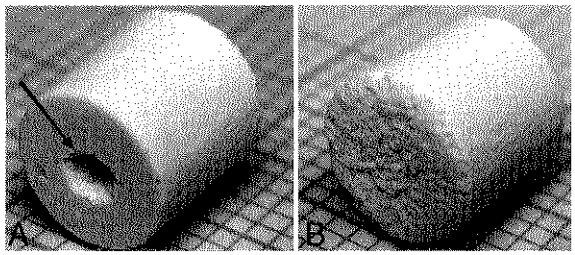

FIG. 5. Cavitation damage to artificial stone. (**A**) Proximal surface of U-30 artificial stone treated with 50 SWs delivered at 20 kV, 0.5 Hz. Cavitation bubble cluster activity has created 2–mm crater centered at proximal end of stone (arrow) (background grid = 1 mm). (**B**) Distal end of stone shows very little damage. There is no focus of erosion, as is seen at proximal end (panel A). Note: Distal ends of U-30 stones are always somewhat rougher than proximal ends, as distal end is not in contact with plastic mold used to cast stone.

when a crack was present in the stone, the side cluster developed along the crack and collapsed into it (Figs. 9 and 10). For example, Figure 9 shows a stone that has a fracture about 3 mm from the distal end. In this set of images, the bubble cluster at the side of the stone formed right on top of the crack (Fig. 9C, D). On collapse, the cluster disappeared into the crack (Fig. 9E). The same cavitation behavior was seen with other stones in which cracks developed at different locations along the side (Figs. 10–12). Thus, superposition of the cluster over the crack did not appear to be a coincidence. That is, it did not matter whether the crack was close to the rubber band (Figs. 10 and 12) or close to the distal end of the stone (Figs. 9 and 11): the cluster still collapsed at the crack.[34] When bubble clusters collapsed into cracks, it often appeared that the cracks became wider (Figs. 9–11). However, it is not clear from analysis of the images whether this bubble activity was directly responsible for widening the gap.

Bubble clusters developed at the surface of natural kidney stones

The formation of cavitation bubble clusters was not limited to situations when artificial stones were used as a target. Figure 12 shows a calcium oxalate monohydrate stone in which a cluster developed over the side and subsequently collapsed along the line of a fracture. Also, in these images, there is a very close correlation between the site of collapse of the side cluster and the location of cracks that developed in the stone.

DISCUSSION

Theoretical models of cavitation and SW–bubble interactions generally assume bubbles to be single, spherical, and relatively small,[13,38,39,41,42] but experimental studies have shown convincingly that such ideal characteristics do not always hold true.[15,32,34,36,42] Our observations with high-speed imaging reiterate these findings and go on to show in greater detail the dynamic nature of cavitation bubble activity at the surface of stones. A key observation from the present study is that the cavitation bubbles that form under the influence of the tensile phase of the SW come to lose their identity as solitary bubbles and merge to form bubble clusters. In other words, the cavitation bubbles that form on the surface of stones do not cycle independently of one another but instead interact as dynamic clusters.

The cavitation we observed to be associated with both artificial and natural stones was characterized by the formation of bubbles that grew to cover large areas of the stone's surface.

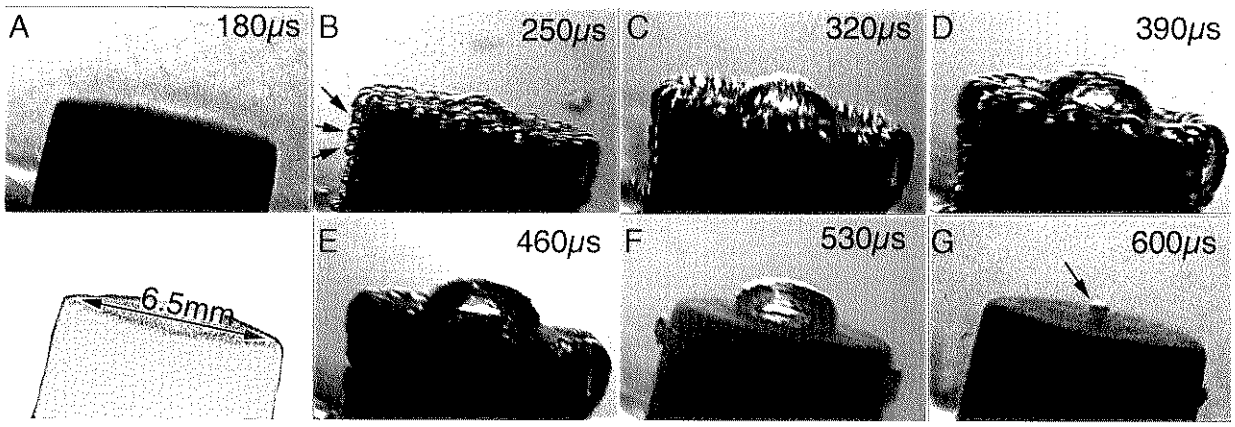

FIG. 6. Cavitation bubble activity at distal third of artificial stone. This is same stone shown in Figure 1 with illumination from different angle. Timing of frames is same (i.e., 70-μsec steps beginning at 180 μsec). (**A**) This frame, included for reference, shows stone at time of SW arrival but before cavitation bubbles have developed. (**B–D**) Formation of individual bubbles and their subsequent growth. Backlighting helps one see boundaries of individual bubbles at edge of stone (arrows) but obscures detail elsewhere. (**E, F**) Bubble cluster atop distal end of stone looks like it may be solitary bubble. At its maximum expansion, this bubble extends slightly more than 1 mm above stone surface. This distal bubble cluster thus is much smaller than cluster that develops at proximal end of stone (see Figs. 2, 3, and 9–11). Structure of this bubble seems very similar to shape attributed to asymmetric bubble collapse.[1] (**G**) Final frame has captured what remains of distal bubble cluster (arrow) as it collapses at center of stone.

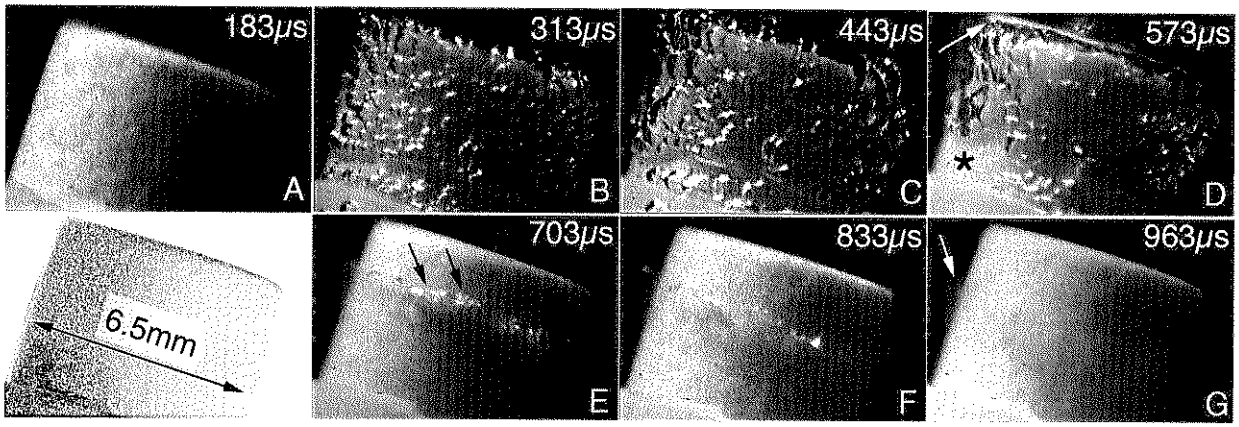

FIG. 7. Bubble cluster formation and collapse at sides of artificial stone. This series of images shows upper (distal) half of stone held in position with rubber band (seen in lower left corner of each frame). Shockwave entered from bottom of stone. Frames were captured in 130-μsec steps. (**A**) At time of SW impact but before bubbles are visible. (**B, C**) Formation and enlargement of bubble cluster that surrounds stone. (**D**) Bubble cluster has begun to retract, exposing midportion (asterisk) and distal edge (white arrow) of stone. (**E, F**) Cluster now forms narrow ring or band of bubbles (black arrows) 1 to 2 mm below distal end. (**G**) In this final frame, there is very faint dust near line of cluster collapse (white arrow), suggestive of fine debris released from stone surface.

These large bubbles tended to be irregular in shape. It generally was not possible to determine whether there was a single cavity of complicated shape or if the cavitation consisted of numerous smaller bubbles. Because the behavior of these bubbles was quite different from what has been appreciated to characterize individual, spherical cavitation bubbles, we have chosen to refer to them as "bubble clusters." Some of the original studies of multiple cavitation bubbles[46,47,62,63] used the term "cavity cluster" for what is now often referred to as "cloud cavitation."[64] The latter is typically associated with a large number of cavitation bubbles that are sufficiently dilute that they do not interact directly (coalesce), even though they may produce large dynamic effects by effectively changing the average properties and dynamics of the fluid as a whole (i.e., bubbles and liquid). The present use of the term "cluster" thus is purely descriptive and is not necessarily meant to imply any close association with the phenomenon of cloud cavitation or its analytical modeling.

Bubble clusters developed consistently in several locations on the stone surface: at the proximal face, along the sides, and at the distal end. It is likely that the size and shape of a stone will influence bubble cluster behavior, and one might expect bubble dynamics to change as the stone is progressively broken into smaller fragments. In our studies with intact stones, the largest bubble cluster formed on the proximal face. Because cavitation bubble expansion is dependent mainly on the amplitude of the tensile phase of the lithotripter SW, bubbles would be expected to grow largest in the region of highest negative pressure. Such a region is the area immediately in front of the

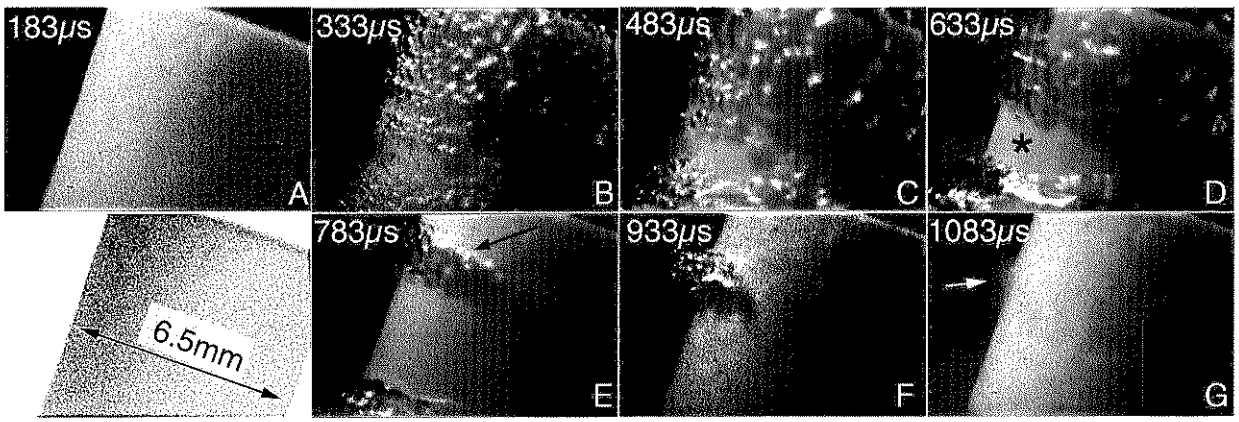

FIG. 8. Bubble cluster formation on artificial stone not held by ligature but rather standing upright atop sheet of low-density polyethylene, demonstrating that formation of bubble cluster at side of stone was not artifact of way stone was held in lithotripter. Frames were captured in 150-μsec steps. (**A**) At time of SW arrival. (**B–F**) Formation of bubble cluster to cover stone surface, retraction of cluster from midportion (asterisk) and distal end to form narrow band of bubbles (black arrow), and collapse of those bubbles. (**G**) As in Figure 6G, this image shows dust (white arrow) that may be fine debris coming from stone surface.

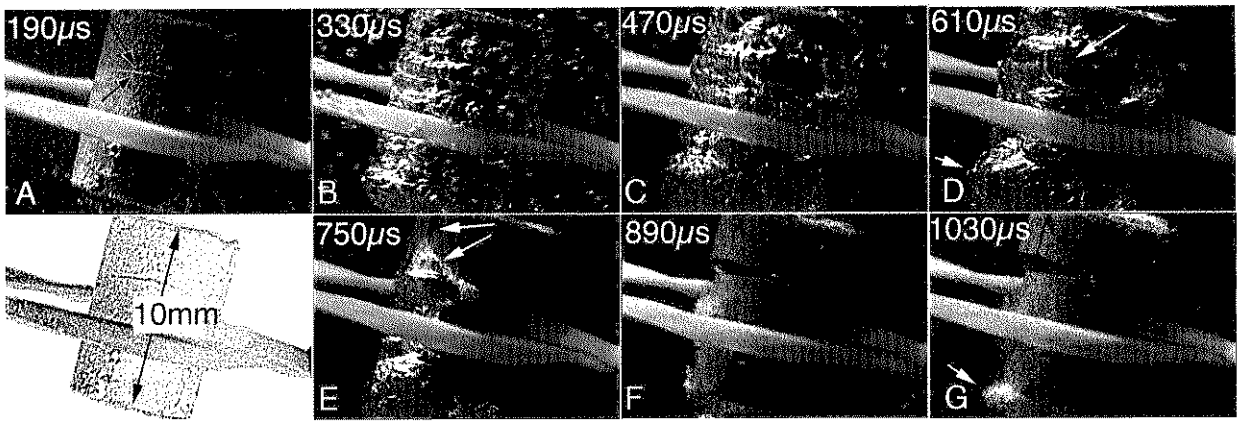

FIG. 9. Bubble cluster collapse along distal spall fracture in artificial stone, photographed in 140-μsec steps. Stone is held in place by rubber band. (**A**) Stone at 190 μsec after spark discharge, approximately 10 μsec later than initial frames in Figures 1, 2, and 6–8. Bubbles are already visible in surrounding water, and some may be present on surface of stone. Transverse crack is visible above rubber band (arrows); this crack was present prior to this shot. (**B, C**) Bubbles grow on surface of stone and coalesce to form large cluster that surrounds most of stone. (**D**) Crack is visible (arrow) beneath cluster at side of stone. Crack appears to have widened. Note also large proximal cluster (arrowhead). (**E**) Bubble cluster at side of stone has collapsed along line of transverse crack. A vertical crack is now visible as well, and portion of cluster overlies this crack (arrows). Proximal cluster is retracting toward leading face of stone. (**F**) Crack is now considerably wider. (**G**) Bubble rebound at proximal face of stone (arrow).

stone. When the pressure pulse impacts the stone, a portion of its energy is reflected. Because the water–stone interface is an acoustically hard boundary, the SW will reflect in phase, and the negative pressure will be increased by ~60%. Cavitation may also be more prominent on the proximal face of a stone because cavitation nuclei might be more abundant in this region. That is, as the proximal face becomes etched and pitted, these outward-facing defects would tend to capture cavitation nuclei.[65,66] The presence of nuclei generated by one pulse could then promote bubble growth during subsequent SWs.[42,67]

The bubble clusters that formed in different locations appear to have contributed to stone breakage in different ways. The proximal cluster typically caused erosion or pitting of the leading face of the stone. For most stones, this damage was prominent. In addition to this direct effect, cluster collapse at the proximal end of the stone likely generated a secondary SW of substantial magnitude. Such a SW originating from cluster collapse could produce pressure gradients within the stone that could contribute to breakage by other mechanisms such as spall.[7,15,54] In related experiments, we have observed that al-

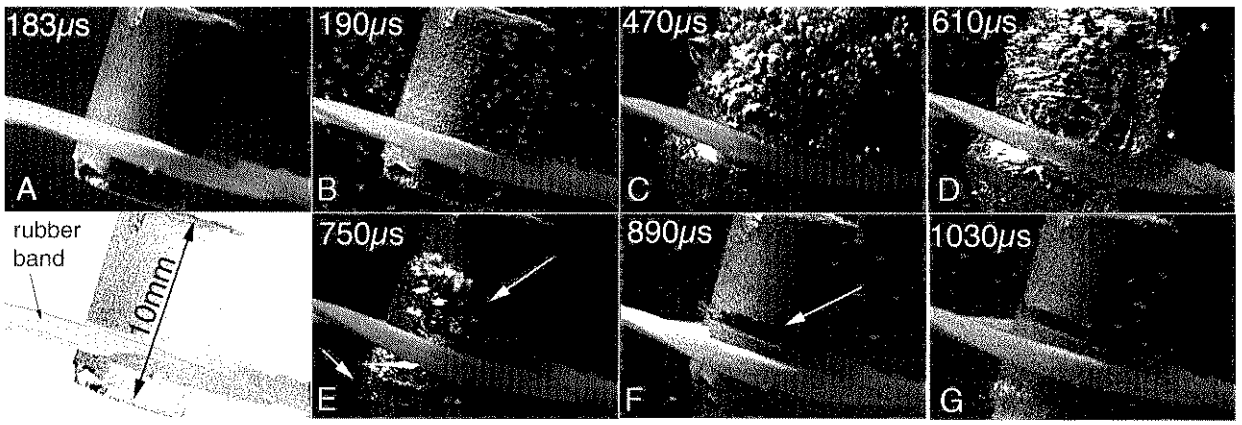

FIG. 10. Superposition of bubble clusters on fracture lines is not accidental. These images are of artificial stone in which spall-type fracture developed low on stone. Bubble cluster still formed along crack and appeared to collapse into it. Steps after panel are at 140 μsec. (**A**) Prior to the arrival of SW. (**B**) Bubbles have begun to form on surface of stone and in surrounding water. (**C, D**) Growth of bubble cluster that appears to surround stone. (**E**) Bubble clusters at side of stone and on proximal end (arrows). Side cluster has narrow portion that runs transversely across stone. One cannot see what lies beneath cluster, but this is position of crack visible in panel F. Thus, bubble cluster appears to be collapsing into crack. (**F, G**) Cluster is gone, and crack is now visible just above rubber band (arrow).

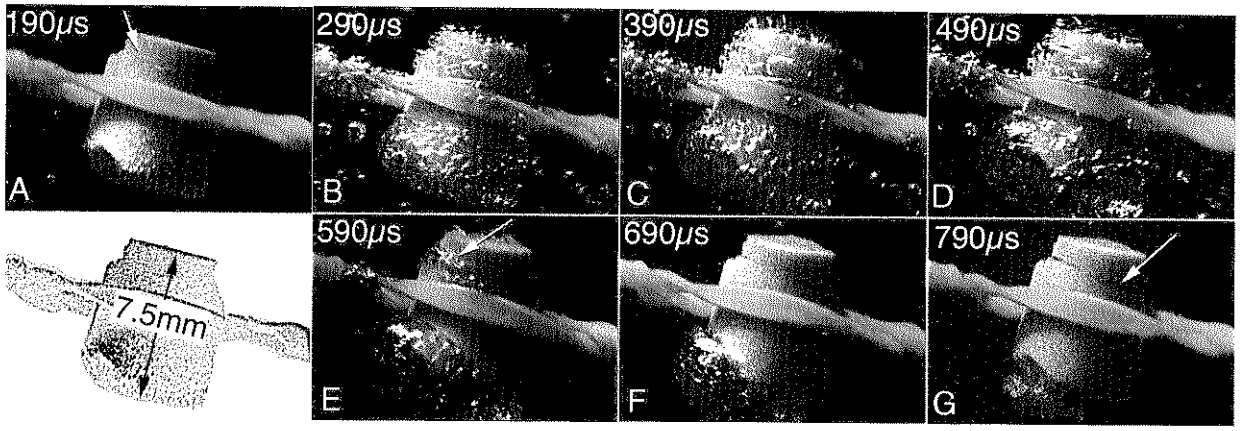

FIG. 11. Bubble cluster activity over different regions of stone captured in 100-μsec steps after single lithotripter pulse. (**A**) Initial frame at 190 μsec shows small bubbles on stone surface and in surrounding water. Stone has already been damaged by previous exposure to SWs. There is faint fracture about 1 mm from distal end (arrow). (**B–D**) Bubbles grow and coalesce to form prominent cluster at proximal end, smaller cluster at distal end, and cluster surrounding midportion. (**E**) Bubbles above rubber band (arrow) are lined up along transverse fracture first visible in panel A. Proximal cluster is very large. (**F**) Proximal cluster is smaller, having begun to collapse. (**G**) Crack near distal end of stone (arrow) has widened, while proximal cluster appears much smaller—consistent with continuation of collapse or subsequent rebound.

though spall fracture of U-30 stones can occur at high overpressure sufficient to inhibit cavitation, distal transverse fracture occurs more readily under conditions that permit cavitation on the proximal face of the stone.[17] These high-speed camera images, which show cluster collapse to be dramatic and tightly focused at the proximal end of stones, lend support to the idea of such a relation between cavitation and spall.

Damage to the distal end of the stones was minor compared with the erosion produced at the proximal end. The bubble clusters that formed on the distal face rarely grew to more than a millimeter in height and occupied a footprint no more than several millimeters in diameter. This compares with proximal clusters that grew to cover, or even overlap, the entire 6.5-mm proximal end of the stone. The shape of the clusters at collapse was also different at the two ends of the stone: whereas the proximal cluster typically formed a mushroom shape (see Fig. 2), the distal cluster sometimes gave the appearance of a single bubble that collapsed asymmetrically. For example, the sequence of frames in Figure 6 shows images that capture the coalescence of small bubbles to form a distal cluster that, just before collapse, appears to contain a vortex. This vortex form has previously been described as a characteristic of the asymmetric bubble collapse that results in focal pitting of metal targets.[1] In the present study, however, the effect of such bubbles on the distal face of the stone was unremarkable.

The collapse of bubble clusters at the sides of stones may have contributed to the growth of fractures. In many cases, the direct damage caused by clusters that encircled the stone was not impressive and appeared to consist of the loss of small amounts of sand that were visible as a faint mist of particles raised off the surface (e.g., see Figs. 7G and 8G). In some instances, however, cluster collapse was associated with the growth of cracks. In almost all cases when a crack was already visible in the stone, the cluster developed and collapsed at that location (e.g., see Figs. 9 and 11). An existing crack might act as a focus for bubble cluster formation by providing a source of cavitation nuclei. A crack might physically stabilize cavitation bubbles,[65,66,68] keeping them from being swept away by fluid motion induced by bubble dynamics elsewhere on the stone. It has also been suggested that cavitation associated with a crack or crevice could produce large tensile stresses during rebound and thereby contribute to crack growth.[51]

These high-speed camera observations do not rule out the possibility that cavitation was involved in the initiation of new fractures. Sass and associates[34] have suggested this as a potential mechanism for SW damage to gallstones. The series of images in Figure 12 (left column) shows a close correlation between the position of cluster collapse and the formation of a crack in a natural stone that does not become obvious until the next shock wave (Fig. 12, right column). Image resolution is a limitation here. It may be that a microscopic fracture existed prior to the first SW and did not grow to visible size until the subsequent shot. What seems most reasonable to conclude is that, overall, the images demonstrate that bubble clusters are associated with fractures in stones and that cluster collapse along the line of a fracture may promote its growth.

Previous studies using high-speed imaging have demonstrated the formation and collapse of cavitation bubbles at the surface of natural and artificial stones. Sass and associates[34] used a high-speed camera system capable of capturing sequential images at 100-μsec steps—comparable to the frame rate we used for the present study. Some of their observations seem to correlate well with our findings. For example, they demonstrate greater bubble activity at the proximal face than elsewhere on the stone, and they suggest that bubbles appeared to fuse at this leading face of the stone. However, the images give no indication of the recruitment of individual bubbles to form aggregates or clusters and do not show evidence of the dynamic movement of bubbles across the surface of the stone that characterized bubble behavior in our experiments. In a recent study, Xi and Zhong[36] used fast-frame photoelastic imaging to capture cavitation bubble activity on the surface of epoxy model stones.

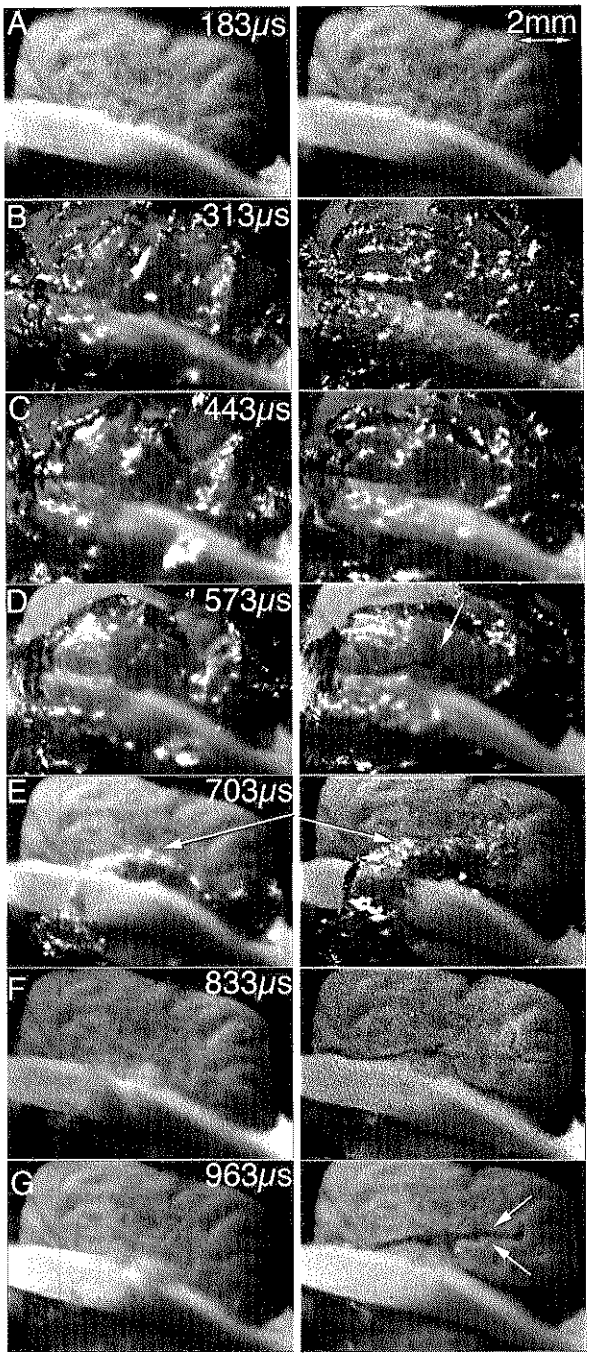

FIG. 12. Cavitation bubble cluster activity on surface of natural calcium oxalate monohydrate kidney stone. Images were obtained after two successive SWs (left column = shot number 3; right column = shot number 4) fired several minutes apart but imaged at same frame rate (130-μsec steps). Reading down, one can see progression of bubble activity during one shot. Reading across, one can compare bubble behavior from one SW to the next. Note similarity of size and location of bubble clusters that formed with each of the two SWs. Note also that bubble cluster collapses along crack that becomes visible after second SW and that crack continues to grow after cluster collapse. (**A**) Stone at time of arrival of SW. (**B, C**) Bubble cluster forms at side of stone, retracts from distal end, and forms band that appears to extend around stone. (**D**) Cluster in 4th shot (right column) overlies prominent crack (arrow) that is first visible in previous frame (**C**). (**E**) Lines of bubble collapse in these two frames are very similar. For shot 4 (right column), location of bubble correlates well with crack visible in earlier frames and easily seen in panels F and G. In shot 3 (left column), no crack is visible, but cluster (arrow) is collapsing along line that seems to correlate well with location of fracture that developed during shot 4. (**F**) At time of collapse of proximal cluster (out of field of view). (**G**) Crack has widened, and segment of this crack (arrows) is now visible after cluster collapse.

They recorded single frames with each lithotripter pulse and staggered the shutter delay time in order to build a sequence over the lifetime of the bubble cycle. These images, with high contrast and good resolution, show two-dimensional profiles of bubble growth on the surface of the blocks. In some sequences, bubbles enlarge and grow to surround the target. Later frames show bubbles primarily at the proximal and distal sides. The images capture profiles in just two dimensions, so it is difficult to appreciate bubble movement; however, the profiles support the idea that bubbles coalesce to cover large areas of the target.

CONCLUSIONS

These observations with high-speed imaging lead to several conclusions about the characteristics of the cavitation associated with stones and the role that cavitation bubbles play in stone fragmentation in SWL. The data show that cavitation bubble activity on the surface of stones *in vitro* is dominated by the formation of bubble clusters. Cluster formation involves the aggregation of many individual cavitation bubbles. Clusters grow and shift dramatically, sweeping across the surface of the stone and collapsing at discrete foci. Separate clusters develop over different regions of the stone and contribute to stone breakage in different ways. The cluster that develops and collapses at the proximal end of the stone is the largest and causes prominent pitting at that leading face. Bubble clusters consistently form also at the distal end of the stone and along the sides. Cluster formation occurs with natural as well as with artificial stones. Cracks that develop in a stone attract bubble cluster activity, and cavitation along an existing fracture may help such fractures to grow. Thus, our observations lend further support to the well-established idea that cavitation contributes to stone comminution through erosion and pitting and also suggest that cavitation bubble cluster activity is involved in the growth of fractures in stones treated by SWL.

ACKNOWLEDGMENT

This research was supported by U.S. National Institutes of Health grants DK43881 and DK55674 and by a grant from the Whitaker Foundation.

REFERENCES

1. Crum LA. Cavitation microjets as a contributory mechanism for renal calculi disintegration in ESWL. J Urol 1988;140:1587–1590.
2. Delius M. Minimal static excess pressure minimises the effect of extracorporeal shock waves on cells and reduces it on gallstones. Ultrasound Med Biol 1997;23:611–617.
3. Sass W, Dreyer HP, Kettermann S, Seifert J. The role of cavitational activity in fragmentation processes by lithotripters. J Stone Dis 1992;4:193–207.
4. Vakil N, Everbach EC. Transient acoustic cavitation in gallstone fragmentation: A study of gallstones fragmented in vivo. Ultrasound Med Biol 1993;19:331–342.
5. Zhong P, Cioanta I, Cocks FH, Preminger GM. Inertial cavitation and associated acoustic emission produced during electrohydraulic shock wave lithotripsy. J Acoust Soc Am 1997;101:2940–2950.
6. Zhong P, Cocks FH, Cioanta I, Preminger GM. Controlled, forced collapse of cavitation bubbles for improved stone fragmentation during shock wave lithotripsy. 1997;158:2323–2328.
7. Zhu S, Cocks FH, Preminger GM, Zhong P. The role of stress waves and cavitation in stone comminution in shock wave lithotripsy. Ultrasound Med Biol 2002;28:661–671.
8. Carstensen EL, Gracewski S, Dalecki D. The search for cavitation in vivo. Ultrasound Med Biol 2000;26:1377–1385.
9. Coleman AJ, Choi MJ, Saunders JE. Detection of acoustic emission from cavitation in tissue during clinical extracorporeal lithotripsy. Ultrasound Med Biol 1996;22:1079–1087.
10. Delius M, Ueberle F, Eisenmenger W. Extracorporeal shock waves act by shock wave-gas bubble interaction. Ultrasound Med Biol 1998;24:1055–1059.
11. Evan AP, Willis LR, McAteer JA, et al. Kidney damage and renal functional changes are minimized by waveform control that suppresses cavitation in SWL. J Urol 2002;168:1556–1562.
12. Sapozhnikov OA, Bailey MR, Crum LA, et al. Ultrasound guided localized detection of cavitation during lithotripsy in pig kidney in vivo. Proc IEEE Ultrasonics Symp 2001;1437–1440.
13. Zhong P, Zhou Y, Zhu S. Dynamics of bubble oscillation in constrained media and mechanisms of vessel rupture in SWL. Ultrasound Med Biol 2001;27:119–134.
14. Vakil N, Gracewski SM, Everbach EC. Relationship of model stone properties to fragmentation mechanisms during lithotripsy. J Lithotrip Stone Dis 1991;3:304–310.
15. Zhong P, Chuong CJ, Preminger GM. Propagation of shock waves in elastic solids caused by cavitation microjet impact II: Application in extracorporeal shock wave lithotripsy. J Acoust Soc Am 1993;94:29–36.
16. Holmer NG, Almquist LO, Hertz TG, Holm A, Lindstedt E, Persson HW, Hertz CH. On the mechanism of kidney stone disintegration by acoustic shock waves. Ultrasound Med Biol 1991;17: 479–489.
17. McAteer JA, Cleveland RO, Rietjens DL, Pishchalnikov YA, Pishchalnikova IV, Williams JC Jr. Cavitation promotes spall failure of model kidney stones treated by shock wave lithotripsy *in vitro*. Proc 17th Int Congress Acoust 2002;VII:188–189.
18. Bailey MR. Acoustic and cavitation fields of a pressure release ellipsoidal reflector [abstract]. J Acoust Soc Am 1997;101:3138.
19. Cathignol D, Tavakkoli J, Birer A, Arefiev A. Comparison between the effects of cavitation induced by two different pressure-time shock waveform pulses. IEEE Trans Ultrason Ferroelectr Freq Control 1998;45:788–799.
20. Bailey MR. Control of acoustic cavitation with application in lithotripsy [Ph.D. thesis]. Technical Report ARL-TR-97-1, Applied Research Laboratories, The University of Texas at Austin, 1997.
21. Sokolov DL, Bailey MR, Crum LA. Use of a dual-pulse lithotripter to generate a localized and intensified cavitation field. J Acoust Soc Am 2001;110:1685–1695.
22. Zhong P, Zhou Y. Suppression of large intraluminal bubble expansion in shock wave lithotripsy without compromising stone comminution: Methodology and *in vitro* experiments. J Acoust Soc Am 2001;110:3283–3291.
23. Bailey MR, Blackstock DT, Cleveland RO, Crum LA. Comparison of electrohydraulic lithotripters with rigid and pressure-release ellipsoidal reflectors II: Cavitation fields. J Acoust Soc Am 1999;106:1149–1160.
24. Coleman AJ, Saunders JE, Crum LA, Dyson M. Acoustic cavitation generated by an extracorporeal shockwave lithotripter. Ultrasound Med Biol 1987;13:69–76.
25. Lifshitz DA, Williams JC Jr, Sturtevant B, Conners BA, Evan AP, McAteer JA. Quantization of shock wave cavitation damage *in vitro*. Ultrasound Med Biol 1997;23:461–471.
26. Delacretaz G, Rink K, Pittomvils G, Lafaut JP, Vandeursen H, Boving R. Importance of the implosion of ESWL-induced cavitation bubbles. Ultrasound Med Biol 1995;21:97–103.
27. Huber P, Debus J, Peschke P, Hahn EW, Lorenz WJ. In vivo detection of ultrasonically induced cavitation by a fibre-optic technique. Ultrasound Med Biol 1994;20:811–825.
28. Coleman AJ, Choi MJ, Saunders JE, Leighton TG. Acoustic emission and sonoluminescence due to cavitation at the beam focus of an electrohydraulic shock wave lithotripter. Ultrasound Med Biol 1992;18:267–281.
29. Coleman AJ, Whitlock M, Leighton T, Saunders JE. The spatial distribution of cavitation induced acoustic emission, sonoluminescence and cell lysis in the field of a shock wave lithotripter. Phys Med Biol 1993;38:1545–1560.
30. Matula TJ, Hilmo PR, Bailey MR, Crum LA. In vitro sonoluminescence and sonochemistry studies with an electrohydraulic shock wave lithotripter. Ultrasound Med Biol 2002;28:1199–1207.
31. Jöchle K, Debus J, Lorenz WJ, Huber P. A new method of quantitative cavitation assessment in the field of a lithotripter. Ultrasound Med Biol 1996;22:329–338.
32. Huber P, Debus J, Jöchle K, et al. Control of cavitation activity by different shockwave pulsing regimes. Physics Med Biol 1999;44: 1427–1437.
33. Cleveland RO, Sapozhnikov OA, Bailey MR, Crum LA. A dual passive cavitation detector for localized detection of lithotripsy-induced cavitation *in vitro*. J Acoust Soc Am 2000;107:1745–1758.
34. Sass W, Braunlich M, Dreyer HP, Matura E, Folberth W, Priesmeyer HG, Seifert J. The mechanisms of stone disintegration by shock waves. Ultrasound Med Biol 1991;17:239–243.
35. Carnell MT, Emmony DC. A schlieren study of the interaction between a lithotripter shock wave and a simulated kidney stone. Ultrasound Med Biol 1995;21:721–724.
36. Xi X, Zhong P. Dynamic photoelastic study of the transient stress field in solids during shock wave lithotripsy. J Acoust Soc Am 2001;109:1226–1239.
37. Vogel A, Busch S, Parlitz U. Shock wave emission and cavitation bubble generation by picosecond and nanosecond optical breakdown in water. J Acoust Soc Am 1996;100:148–165.
38. Choi MJ, Coleman AJ, Saunders JE. The influence of fluid properties and pulse amplitude on bubble dynamics in the field of a shock wave lithotripter. Phys Med Biol 1993;38:1561–1573.
39. Church CC. A theoretical study of cavitation generated by an extracorporeal shock wave lithotripter. J Acoust Soc Am 1989;86: 215–227.
40. Ding Z, Gracewski SM. Response of constrained and unconstrained bubbles to lithotripter shock wave pulses. J Acoust Soc Am 1994;96:3636–3644.
41. Matula TJ, Hilmo PR, Storey BD, Szeri AJ. Radial response of individual bubbles subjected to shock wave lithotripsy pulses *in vitro*. Physics Fluids 2002;14:913–921.
42. Sapozhnikov OA, Khokhlova VA, Bailey MR, Williams JC Jr, McAteer JA, Cleveland RO, Crum LA. Effect of overpressure and

pulse repetition frequency on cavitation in shock wave lithotripsy. J Acoust Soc Am 2002;112:1183–1195.
43. Zhu S, Zhong P. Shock wave–inertial microbubble interaction: A theoretical study based on the Gilmore formulation for bubble dynamics. J Acoust Soc Am 1999;106:3024–3033.
44. Kodama T, Takayama K. Dynamic behavior of bubbles during extracorporeal shock-wave lithotripsy. Ultrasound Med Biol 1998; 24:723–738.
45. Lauterborn W, Ohl CD. Cavitation bubble dynamics. Ultrasonics Sonochem 1997;4:65–75.
46. Morch KA. On the collapse of cavity clusters in flow cavitation. In: Lauterborn W (ed): Cavitation and Inhomogeneities in Underwater Acoustics. New York: Springer-Verlag, 1980, pp 95–100.
47. Morch KA. Cavity cluster dynamics and cavitation erosion. Proc ASME Cavitation Polyphase Flow Forum 1981:1–10.
48. Omta R. Oscillations of a cloud of bubbles of small and not so small amplitude. J Acoust Soc Am 1987;82:1018–1033.
49. Reisman GE, Wang YC, Brennen CE. Observations of shock waves in cloud cavitation. J Fluid Mech 1998;355:255–283.
50. Smereka P, Banerjee S. The dynamics of periodically driven bubble clouds. Phys Fluids 1988;31:3519–3541.
51. Field JE. The physics of liquid impact, shock wave interactions with cavities, and the implications to shock wave lithotripsy. Phys Med Biol 1991;36:1475–1484.
52. Tanguay M, Colonius T. Numerical investigation of bubble cloud dynamics in shock wave lithotripsy. Proc ASME Fluids Eng Div 2002;FEDSM2002–31010.
53. Cleveland RO, Bailey MR, Hartenbaum B, Lokhandwalla M, McAteer JA, Sturtevant B. Design and characterization of a research electrohydraulic lithotripter patterned after the Dornier HM3. Rev Scientific Instr 2000;71:2514–2525.
54. Gracewski SM, Dahake G, Ding Z, Burns SJ, Everbach EC. Internal stress wave measurements in solids subjected to lithotripter pulses. J Acoust Soc Am 1993;94:652–661.
55. Heimbach D, Munver R, Zhong P, Jacobs J, Hesse A, Muller SC, Preminger GM. Acoustic and mechanical properties of artificial stones in comparison to natural kidney stones. J Urol 2000;164: 527–544.
56. McAteer JA, Cleveland RO, Paterson RF, et al. Evidence that cavitation and spall contribute to stone failure in an animal model of kidney stone fragmentation by shock wave lithotripsy (SWL). Proc 17th Int Congress Acoust 2002;VII:202–203.
57. McAteer JA, Paterson RF, Lifshitz DA, Lingeman JE, Rietjens DL, Connors BA, Evan AP, Williams JC Jr. *In vitro* model of shock wave lithotripsy (SWL) produces stone breakage equivalent to that seen in vivo. Proc 17th Int Congress Acoust 2002;VII:180–182.
58. Paterson RF, Lifshitz DA, Lingeman JE, et al. Slowing the pulse repetition frequency in shock wave lithotripsy (SWL) improves stone fragmentation in vivo. Proc 17th Int Congress Acoust 2002;VII:200–201.
59. Cleveland RO, McAteer JA, Muller R. Time-lapse nondestructive assessment of shock wave damage to kidney stones *in vitro* using micro-computed tomography. J Acoust Soc Am 2001;110: 1733–736.
60. Cleveland RO, McAteer JA, Williams JC Jr. Correlation between the predicted stress field and observed spall-failure in artificial kidney stones treated by shock wave lithotripsy (SWL) in vitro. Proc 17th Int Congress Acoust 2002;VII:174–175.
61. Zhong P, Preminger GM. Mechanisms of differing stone fragility in extracorporeal shockwave lithotripsy. J Endourol 1994;8:263–268.
62. Dear JP, Field JE. A study of the collapse of the arrays of cavities. J Fluid Mech 1988;190:409–425.
63. Hansson I, Morch KA. The dynamics of cavity clusters in ultrasonic (vibratory) cavitation erosion. J Appl Phys 1980;51: 4651–4658.
64. Brennen CE. Cavitation and Bubble Dynamics. Oxford University Press, 1985.
65. Bailey MR, Cleveland RO, Sapozhnikov OA, McAteer JA, Williams JC Jr, Crum LA. Effect of increased ambient pressure on lithotripsy-induced cavitation in bulk fluid and at solid surfaces. J Acoust Soc Am 1999;105:1267–1270.
66. Cleveland RO, Bailey MR, Crum LA, Stonehill MA, Williams JC Jr, McAteer JA. Effect of overpressure on dissolution and cavitation of bubbles stabilized on a metal surface. Proc 135th Acoust Soc Am 1998;4:2499–2500.
67. Delius M, Brendel W. A model of extracorporeal shock wave action: Tandem action of shock waves. Ultrasound Med Biol 1988;14:515–518.
68. Crum LA. Tensile strength of water. Nature 1979;278:148–149.

Address reprint requests to:
James A. McAteer, Ph.D.
Dept. of Anatomy and Cell Biology
Indiana University School of Medicine
635 Barnhill Drive (MS 5055)
Indianapolis, IN 46202-5120

E-mail: mcateer@anatomy.iupui.edu